JOURNAL OF PROPULSION AND POWER
Vol. 19, No. 1, January–February 2003

Thrust-Vectoring Nozzle Performance Modeling

Erich A. Wilson,* Dan Adler,† and Pinhas Bar-Yoseph‡
Technion—Israel Institute of Technology, 32000 Haifa, Israel

A polytropic analytical equation system for the internal flow of nozzles, inlets, and ducts has been developed through an analysis of the compressible flow equations including the friction and area change driving potentials. These equations are verified through comparison with experimental data and numerical simulations using FLUENT 5.0. The nozzle performance predictions include consideration of the nozzle divergence and surface roughness. It is demonstrated that the analytical model well matches the experimental data after the throat is fully choked. The numerical and analytical results are compared and discussed. Such an analytical model is extremely useful in bridging the gap between accepted empirical parameters such as the friction factor, performance coefficients, and analytical performance modeling. Furthermore, it provides the first analytical model for thrust-vectoring nozzle performance predictions. In aircraft nozzle simulations where empirical data may not be available, this model provides good simulation capability.

Nomenclature

A	=	area, m^2
C_D	=	discharge flow coefficient
C_{fg}	=	thrust coefficient
C_v	=	velocity coefficient
C_μ, $C_{1\varepsilon}$, $C_{2\varepsilon}$	=	turbulence constants
d	=	diameter, m
f	=	friction factor
I	=	impulse function, N
k	=	turbulent kinetic energy
M	=	Mach number
$\dot{m}$	=	flow rate, kg/s
p	=	pressure, Pa
p_0	=	stagnation pressure, Pa
R	=	gas constant for air, kJ/(kg · K)
r	=	radius, m
T	=	temperature, K
T_0	=	stagnation temperature, K
u, v, w	=	Cartesian velocity components, m/s
$\boldsymbol{V}$	=	vectoral velocity, m/s
x, y, z	=	Cartesian coordinates
x^G	=	geometric expansion length, m
α	=	nozzle divergence angle, rad
β	=	nozzle convergent angle, rad
Γ	=	$\gamma(f + 2\tan\beta)/2\phi$
γ	=	ratio of specific heats
δ	=	vectoring angle, rad
ε	=	roughness height, m
ζ	=	$1 + (\gamma - 1)/2 \times M^2$
κ	=	analytic term, $\{2\tan(\alpha) - f[1 + (\gamma - 1)M^2]\}/\psi$
λ	=	analytic term, $[(f\gamma + 2\tan\beta)/2\phi]$
ρ	=	density, kg/m^3
ϕ	=	analytic variable, $[f\gamma + (\gamma - 1)\tan\beta]$
ψ	=	$2\tan\alpha - f\gamma M^2$

Subscripts

a	=	actual
e	=	exit
i	=	isentropic, ideal
in	=	nozzle inlet
1	=	arbitrary upstream nozzle station
2	=	arbitrary downstream nozzle station

Superscripts

E	=	effective
G	=	geometric

Introduction

WITH the dawning of thrust-vectoring jet deflection technology, the nozzle design field has increased in scope and application. This technology has been well demonstrated in the F-15, F-16, F-18, and X-31 experimental aircraft, as well as the F-22 and Su-37 production aircraft. Researchers are pursuing ways to both maximize thrust-vectoring nozzle effectiveness[1] in fighter aircraft and apply this technology to civil aircraft.[2]

The dynamic requirements of thrust-vectoring nozzles complicate modeling beyond the standard variables encountered with conventional nozzles.[3] One such complication is the inclusion of the variation in nozzle geometry with its influences on the jet flow.[4] As the nozzle capabilities are expanded, however, fundamental concepts and direct correlations in nozzle performances will allow even further advancements.

New nozzle capabilities require more precise correlation and more seamless transitions between the current design technologies. These technologies generally include a combination of empirical, numerical, and analytical design. In reality, gaps between these methods exist that are most often compensated for by the experience of talented engineers and designers.

The largest fundamental gap between design methods is the correlation between empirical performance parameters and modeling those performances through the compressible flow equations. Current practice calls for filling this gap with empirical performance coefficients that relate the calculations to actual performances. Filling this gap with an analytical solution would build a solid foundation for the future modeling of dynamic thrust-vectoring nozzles. One attempt to bridge this gap has been made[5] with less than definitive results using Young's model.[6]

A similar attempt to bridge the gap is reported by Rebolo et al.[7] They also saw the need for a more refined analytical equation model in nozzle design and development. In their development model, they obtain very good matching with experimental data. However, they resorted to empirical data to adjust the ideal equations and obtain

Received 28 April 2001; revision received 27 July 2001; accepted for publication 4 September 2002.

*Graduate Student, Faculty of Mechanical Engineering.
†Professor and Head of the Turbo Machinery Laboratory, Faculty of Mechanical Engineering.
‡Professor and Head of the Computational Mechanics Laboratory, Faculty of Mechanical Engineering.

the nozzle performance prediction, and so a pure analytical model was not attained.

A polytropic equation system developed by the present authors as a solution to the combined friction/area change compressible flow is implemented in this work. This equation system serves as a basis for the analytical equations given here to predict the nozzle performance coefficients through analytical means. The prediction capability of the polytropic analytical model is compared with three-dimensional numerical simulations using FLUENT 5.0 and experimental data.[8]

For practical geometrical purposes, the polytropic equation system considers only axisymmetric converging–diverging nozzles. Transformation to two-dimensional nozzles is simply undertaken through developing the cross-sectional area term from the product of the height and length of the nozzle just as the area development here is pursued for a circular to elliptic nozzle cross section.

Thus, this work seeks to bride the gap between empirical data and system modeling by providing an analytical system to predict actual performances in thrust-vectoring nozzles.

Analytic Solution for Combined Friction/Area Change Compressible Flow

Application of the compressible flow equations in nozzles allows the generalized differential equations to be reduced to two driving potential terms, the area change and the friction. The entire equation system is given the first column in Table 1. The analytic solutions to this equation set are achieved through a transformation of the two driving functions to functions based on nozzle length x, as shown in the middle column of Table 1. For this transformation, the area term

Table 1 Summary of equations for flows with area change and friction

General equation differential form	Compact differential form	Property ratios
$\frac{dM^2}{M^2} = -\frac{2\zeta}{1-M^2}\frac{dA}{A} + \frac{\gamma M^2 \zeta}{1-M^2}\frac{4f}{D}dx$	$\frac{dA}{A} = -\frac{1-M^2}{2\zeta\{1-(\gamma M^2/2)[f/\tan(\alpha)]\}}\frac{dM^2}{M^2}$	$\frac{A_2}{A_1} = \frac{M_1}{M_2}\left(\frac{\zeta_2}{\zeta_1}\right)^{(\gamma+1)\tan(\alpha)/2\phi}\left(\frac{\psi_2}{\psi_1}\right)^{[f\gamma-2\tan(\alpha)]/2\phi}$
$\frac{dV}{V} = -\frac{1}{1-M^2}\frac{dA}{A} + \frac{\gamma M^2}{2(1-M^2)}\frac{4f}{D}dx$	$\frac{dV}{V} = \frac{1}{2\zeta}\frac{dM^2}{M^2}$	$\frac{V_2}{V_1} = \frac{M_2}{M_1}\left(\frac{\zeta_1}{\zeta_2}\right)^{\frac{1}{2}}$
$\frac{dT}{T} = \frac{(\gamma-1)M^2}{1-M^2}\frac{dA}{A} - \frac{\gamma M^4(\gamma-1)}{2(1-M^2)}\frac{4f}{D}dx$	$\frac{dT}{T} = -\frac{(\gamma-1)M^2}{2\zeta}\frac{dM^2}{M^2}$	$\frac{T_2}{T_1} = \frac{\zeta_1}{\zeta_2}$
$\frac{d\rho}{\rho} = \frac{M^2}{1-M^2}\frac{dA}{A} - \frac{\gamma M^2}{2(1-M^2)}\frac{4f}{D}dx$	$\frac{d\rho}{\rho} = -\frac{M^2}{2\zeta}\frac{2\tan(\alpha)-f\gamma}{\psi}\frac{dM^2}{M^2}$	$\frac{\rho_2}{\rho_1} = \left(\frac{\zeta_1}{\zeta_2}\frac{\psi_1}{\psi_2}\right)^{[f\gamma-2\tan(\alpha)]/2\phi}$
$\frac{dP}{P} = \frac{\gamma M^2}{1-M^2}\frac{dA}{A} - \frac{\gamma M^2[1+(\gamma-1)M^2]}{2(1-M^2)}\frac{4f}{D}dx$	$\frac{dP}{P} = -\frac{\gamma M^2}{2\zeta}\kappa\frac{dM^2}{M^2}$	$\frac{P_2}{P_1} = \left(\frac{\zeta_1}{\zeta_2}\right)^{\gamma[f+2\tan(\alpha)]/2\phi}\left(\frac{\psi_1}{\psi_2}\right)^{[f\gamma-2\tan(\alpha)]/2\phi}$
$\frac{dP_0}{P_0} = -\frac{\gamma M^2}{2}\frac{4f}{D}dx$	$\frac{dP_0}{P_0} = \frac{\gamma M^2 f(1-M^2)}{2\psi\zeta}\frac{dM^2}{M^2}$	$\frac{P_{02}}{P_{01}} = \left(\frac{\zeta_2}{\zeta_1}\right)^{f\gamma(\gamma+1)/2(\gamma-1)\phi}\left(\frac{\psi_2}{\psi_1}\right)^{-[f\gamma-2\tan(\alpha)]/2\phi}$
$\frac{dT_0}{T_0} = 0$		$T_0 = \text{const}$
$\frac{ds}{c_p} = \frac{(\gamma-1)M^2}{2}\frac{4f}{D}dx$	$\frac{ds}{c_p} = -\frac{(\gamma-1)M^2 f}{2\zeta}\frac{1-M^2}{\psi}\frac{dM^2}{M^2}$	$\frac{\Delta s}{c_p} = \ln\left\{\left(\frac{\zeta_1}{\zeta_2}\right)^{f(\gamma+1)/2\phi}\left(\frac{\psi_2}{\psi_1}\right)^{[(\gamma-1)/\gamma][f\gamma-2\tan(\alpha)]/2\phi}\right\}$
$\frac{dI}{I} = \frac{1}{1+\gamma M^2}\frac{dA}{A} - \frac{\gamma M^2}{2(1+\gamma M^2)}\frac{4f}{D}dx$	$\frac{dI}{I} = -\frac{1-M^2}{1+\gamma M^2}\frac{1}{2\zeta}\frac{dM^2}{M^2}$	$\frac{I_2}{I_1} = \frac{M_2}{M_1}\left(\frac{1+\gamma M_2^2}{1+\gamma M_1^2}\right)\left(\frac{\zeta_2}{\zeta_1}\right)^{-\frac{1}{2}}$
0	$\frac{4f}{D}dx = -\frac{f}{2\zeta}\frac{1-M^2}{\psi}\frac{dM^2}{M^2}$	$\frac{4f(x_2-x_1)}{D} = \ln\left\{\left(\frac{\zeta_2}{\zeta_1}\right)^{f(\gamma+1)/2\phi} \times \left(\frac{\psi_2}{\psi_1}\right)^{f[f\gamma-2\tan(\alpha)]/2\phi\tan(\alpha)}\left(\frac{M_1}{M_2}\right)^{f/\tan(\alpha)}\right\}$

s defined as a function of the nozzle divergence angle, local radius, and nozzle length. The friction term, as a function of x, can then be defined as a function of the local area. The development of these transformations are given subsequently. The analytic solutions for the entire equation system are given in the last column of Table 1.

Area Considerations

Consider that throat of the axisymmetric nozzle to be at the origin along body axis x. Thus, any given cross-sectional area of the nozzle can be referenced to the nozzle throat radius r_0 through the divergence angle, which becomes negative if the duct is converging toward the throat,

$$A = \pi\{r_0 + x\tan[f(\alpha)]\}^2 \tag{1}$$

Here, $f(\alpha)$ describes the behavior of the divergence angle along the length of the nozzle. When the derivative along the nozzle length as well as a variational divergence angle are considered, the differential form of Eq. (1) is

$$\mathrm{d}A = 2\pi\{r_0 + x\tan[f(\alpha)]\}(\tan[f(\alpha)]\,\mathrm{d}x + x\,\mathrm{d}\{\tan[f(\alpha)]\}) \tag{2}$$

For practical purposes, Eq. (2) causes great difficulty for the analytic integration system. A simplification for Eq. (2) is to observe that for a small $\mathrm{d}x$, $\mathrm{d}x \gg d\{\tan[f(\alpha)]\}$. This allows the differential term to be neglected while still providing the potential for handling a constant, linear, or parabolically variational divergence angle. With this assumption, Eqs. (1) and (2) allow the differential form of the area variation to be written as a function of the cross-sectional location along the nozzle length in a fairly simple form

$$\frac{\mathrm{d}A}{A} = \frac{2\tan[f(\alpha)]}{r_0 + x\tan[f(\alpha)]}\,\mathrm{d}x \tag{3}$$

For simplicity, the $f(\alpha)$ term will solely be referred to as α throughout the remainder of this paper.

Friction Considerations

Unique to the combination of area change with friction flow is that both differentials of the driving potentials are reducible to a variational function of the location along the body axis x. This characteristic is also mentioned by Young[6] in a similar effort to solve the generalized compressible flow equations.

As a direct consequence to this, the friction term can be written as a function of the area variational. Young's model[6] assumes that the nozzle diameter is linear, which is not always the case, and develops the friction term $4f\,\mathrm{d}x/D = (2f/m)\,\mathrm{d}A/A$. The major restriction to Young's model is that the nozzle divergence angle is excluded and assumed to be constant. This excludes the modeling of all nozzles with parabolic expansion characteristics such as those seen in rockets.

Independent to Young's development, this work has produced a form of the friction factor in terms of the divergence angle α, which is described in Eqs. (1) and (2) as constant, linear, parabolic, or higher order. Thus, $f(\alpha) = f(x)$ can be a constant, $\alpha = \text{const}$ (as in aircraft nozzles); linear $\alpha = f(x)$ (as in rocket nozzles); or parabolic, $\alpha = f(x^2)$, as desired. This option is unavailable in Young's formulation.

In this work, the diameter is always described in terms of its relation to the nozzle throat radius instead of as a linear function. This is a more robust view to take of the nozzle geometry allowing for area variation along the length of the nozzle. Thus,

$$\frac{4f}{D}\,\mathrm{d}x = \frac{1}{2}\frac{[2\tan(\alpha)]}{[2\tan(\alpha)]}\frac{4f}{r_0 + x\tan(\alpha)}\,\mathrm{d}x = \frac{f}{\tan(\alpha)}\frac{\mathrm{d}A}{A} \tag{4}$$

Analytic Friction Modeling

To produce a robust analytical model and to enable an analytical calculation of the performance coefficients, one must consider the effects of friction through surface roughness, as well as the area change throughout the nozzle on the jet flow.

In the case of fully developed, incompressible isothermal flow along a duct, the friction factor has an average invariant value dependent on the Reynolds number and relative roughness. The Moody diagram, created in 1944 from empirical data, is generally an acceptable graphical representation for frictional effects.

Shapiro[8] suggests that, for subsonic flows in nozzles, the low Mach number dependence of the friction factor is unimportant. This is due to the relatively small gradients encountered along the nozzle length where friction has little or no effect.

In compressible supersonic flow, frictional effects are greatly complicated, and the addition of Mach number as an important dimensionless parameter must be included. For flow through the divergent sector of a nozzle, large gradients exist, and frictional points help to trigger and determine the position of shock and expansion waves. No definitive work on the behavior of the friction factor in convergent–divergent nozzles has been published. The usual procedure for compressible flow is to use the Moody diagram or a functional equation form, such as the Colebrook formula (see Ref. 9)

$$f = 0.25\Bigg/\left(\log_{10}\left[\frac{\varepsilon/D}{3.70} + \frac{2.51}{Re\sqrt{f}}\right]\right)^2 \tag{5}$$

Then, the friction factor is evaluated using the Reynolds number definition at each calculated point along the nozzle when

$$Re = \rho VD/\mu = VD/\nu \tag{6}$$

and the relative roughness ε/D. For subsonic flows, especially in ducts, the product of ρV is constant at any location along the duct. For a nozzle or inlet of varying area, this principle is extrapolated such that the viscosity is evaluated as a function of the mean static temperature at a given cross section assumed to be constant for a small $\mathrm{d}x$ value.

Numerical Calculation Method

A numerical investigation using FLUENT 5.0 was carried out to further validate the analytical model over the same range and conditions as the experiments. Each case was solved for a 10^{-4} convergence on all of the residuals including continuity, momentum, energy, and turbulence. These convergence criteria were carried over to the performance coefficients as well. Second-order approximations for pressure with second-order upwind-based approximations for momentum, energy, and turbulence were used. The pressure–velocity coupling was solved using the SIMPLE algorithm.

The turbulence model implemented is the renormalized group k–ε (RNG k–ε) model available with the FLUENT 5.0 code.[10] A comparison with the Reynolds stress model (RSM) showed that numerical deviations were only found in the fifth decimal place of the exit Mach number predicted under the same operating conditions for each model. This is viable because no significant flow separation exists in the conventional nozzles. Thus, the two-equation RNG k–ε model was chosen over the seven-equation RSM to lower the computational requirements.

Definition of turbulence intensity and length scale was preferred on the inlet and exit boundaries of the flowfield as opposed to direct definition of the k and ε values. It was found that the exit Mach number only varied in the fifth decimal place for turbulence intensities ranging from 0.5 to 10%. Supersonic flows in a diverging duct are not turbulent. Thus, the turbulence intensity was arbitrarily chosen to be 5% for both the inlet and the exit. The length scale was chosen to be $l = 0.07d$, where d is the nozzle exit diameter.

Flow boundary conditions were determined as a function of the nozzle pressure ratio (NPR). In this case, the exit pressure remained at ambient while the inlet pressure was raised to obtain the various NPR levels demonstrated in this study. This method provides a plug-type inlet velocity profile in the converging sector of the nozzle.

An initially uniform three-dimensional unstructured grid was used for each model with approximately 10,000 initial nodes for each nozzle configuration, as shown in Fig. 1. Throughout the computations, the grids were adapted for each case according to the velocity gradient to achieve grid of approximately 140,000 nodes. Adaptations along the boundary allowed for proper expansion and shock wave capturing. Grid independence for the performance coefficients was generally achieved above 100,000 nodes.

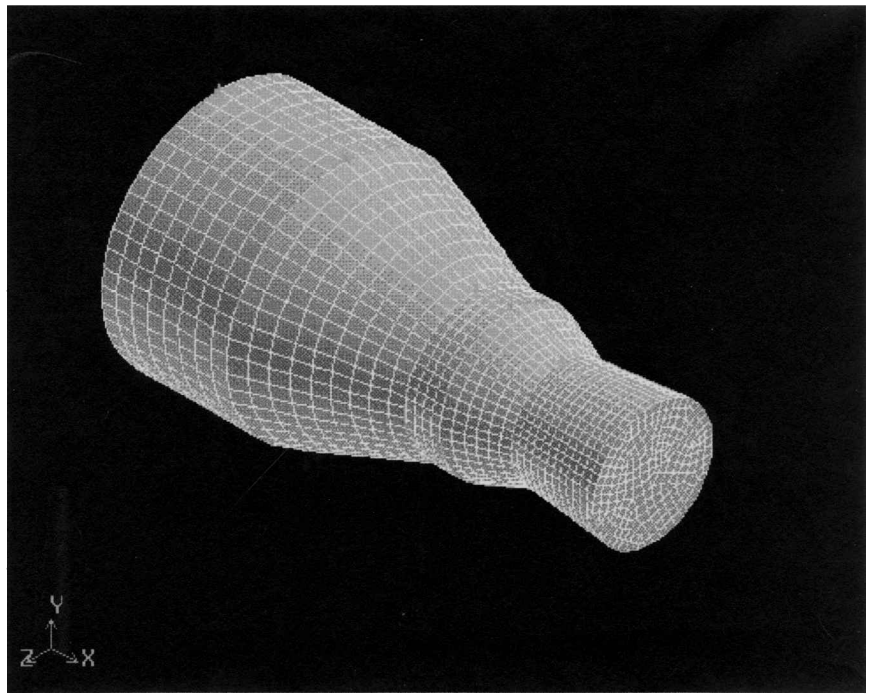

Fig. 1 Initial unstructured grid for the nozzle configuration of Carson and Capone.[11]

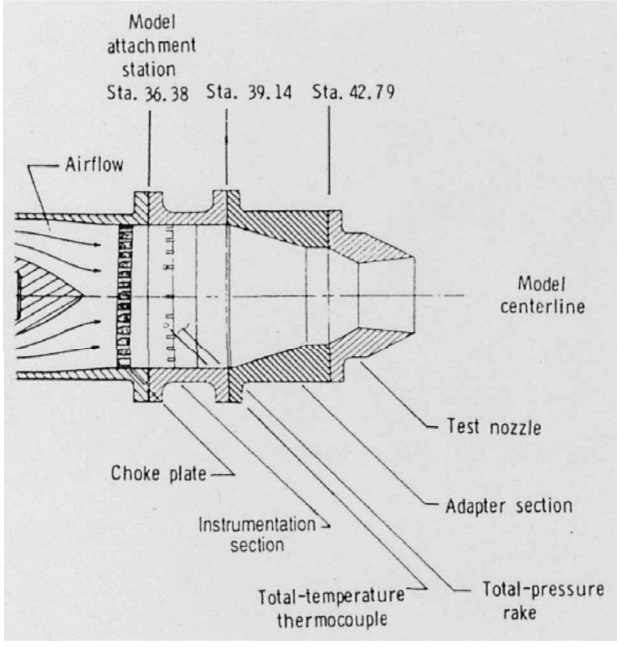

Fig. 2 Experimental setup of Carson and Capone.[11]

Experimental Setup

The nozzle evaluated in this work is the long-length nozzle (0.076-m flap length) configuration from Carson and Capone.[11] Both nozzles have a design area ratio of $A_e/A_t = 1.35$ and a throat area of $A_t = 0.0026$ m^2. Figure 2 shows a schematic diagram of the experimental setup with the unvectored nozzle attached.

The nozzle was machined to a maximum surface roughness of 30 μm, and the actual surface roughness ideally reached about 15 μm. The nozzle was tested at various NPR ($= P_{\text{in}}/P_{\text{out}}$) values ranging from 1.5 up to 8. The discharge flow coefficient C_D and thrust coefficient C_{fg} were measured and recorded. No data on the velocity and angularity coefficients were available. The uncertainty of the data is about $\pm 5\%$.

Table 2 Reduction of effective areas with throat fixed

Area	$\delta_y^G = 0$ deg	$\delta_y^G = 10$ deg	$\delta_y^G = 20$ deg	$\delta_y^G = 30$ deg
A_t^E, m^2	0.0026	0.0025	0.0025	0.0023
	0	9	0	4
Percent reduction, %	0	0.4	4	10
A_e^E/A_t^E	1.350	1.307	1.283	1.260
Percent reduction, %	0	3	5	7

Thrust-Vectoring Nozzle Performances

The performance characteristics of thrust-vectoring nozzles are given as purely analytical functions for the first time as based on the polytropic equation system. In the open literature authors such as Gal-Or,[12] Oates,[13] and Mattingly et al.[14] offer nozzle performance characteristic based on empirical coefficients.

Figure 3 shows a basic schematic diagram of a typical thrust-vectoring nozzle and defines the differences between the geometric and effective parameters. This serves as a basis for determining the thrust-vectoring nozzle performances.

The primary factor that differentiates thrust-vectoring nozzle design from that of conventional nozzle design and that calls for a serious expansion of the design paradigm is the capability of geometric flexibility. Until now, two basic controls for convergent–divergent nozzles were in general practice, fixed-geometry and variable-geometry nozzles. These are still valid control terms in that they refer only to the geometrical throat of the nozzle. However, a much broader definition is that a fixed-geometry nozzle is completely fixed and immovable and a variable geometry can be anything from a variable throat to a complete geometrically dynamic yaw–pitch–roll thrust-vectoring nozzle.

Observe some of the geometrical dynamics that occur. Table 2 shows the geometrical behavior of the effective throat during vectoring as well as the effective area ratio when the geometrical (physical) nozzle throat is held at a constant area. Note how the reduction of the effective throat area tends to be exponential as the vectoring angle is increased, whereas the reduction in effective areas tends to be linear. That both are reduced is logical. If the effective area is

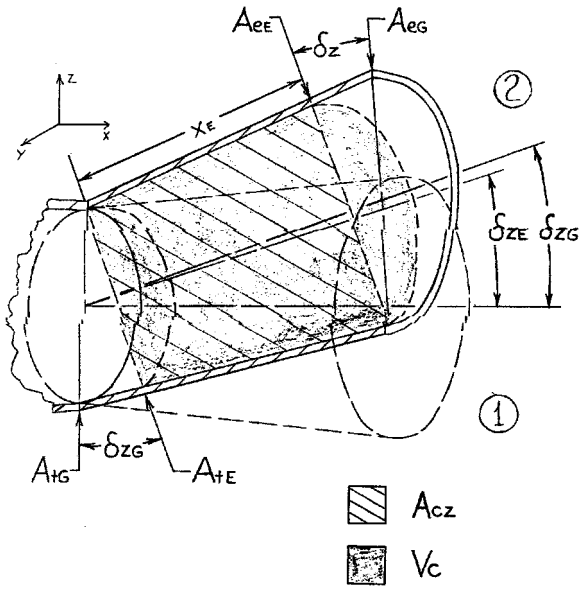

Fig. 3 Schematic of a typical thrust-vectoring nozzle.

increased while the effective throat is decreased, the estimation of the nozzle performances will be divergent in precision.

Further considerations that were not taken in this work and will ultimately determine the capability of calculating the effective vectoring angle as a function of the NPR are concerned with the vena contracta control of the throat and the exit on the flow system. That is, that the effective throat, which moves slightly downstream from the geometric throat and shifts as a function of the geometric vectoring of the nozzle, will surpass the minimum diameter of the throat. Thus, it may be found on further investigation that a minimum diameter lies at some location between the geometric and effective throats. Thus, it may also be postulated that a minimum diameter exists for the nozzle exit that lies slightly upstream from the effective exit. It is still the opinion of the authors that the position of the effective exit determines the effective vectoring angle. The fluctuation of the effective exit angularity as a function of the NPR has not been achieved here and is left for future investigation.

Performance Coefficients

In light of the development of the polytropic system, the actual performances can be estimated and compared to the ideal isentropic calculations to produce expected nozzle performance coefficients through a desired NPR range for any given nozzle design.

Conventional Flow Coefficient

The flow coefficient C_D is the ratio of the actual mass flow rate $\dot{m}_a$ at the throat of the nozzle over the ideal mass flow rate $\dot{m}_i$ at the inlet of the nozzle. Calculating the ideal mass flow can be achieved through the inlet conditions according to

$$\dot{m}_i = \frac{p_0 A_{\text{in}} M_{\text{in}}}{\zeta_{\text{in}}^{(\gamma+1)/2(\gamma-1)}} \sqrt{\frac{\gamma}{RT_0}} \tag{7a}$$

where

$$\zeta = \{1 + [(\gamma - 1)/2]M^2\} \tag{7b}$$

Equation (7) can also be adjusted to calculate the flow rate at the throat under choking conditions. In this case it is written using the geometric throat area

$$\dot{m}_i = 0.6847 p_0 A_t^G \Big/ \sqrt{RT_0} \tag{8}$$

Development of the polytropic flow rate is also of interest to obtain an estimation of the actual flow rate. Beginning with the flow rate equation and substituting in the ideal gas equation achieves

$$\dot{m}_a = \rho V A = \left[(p/RT) M A \sqrt{\gamma RT}\right]_2^E \tag{9}$$

where 2 describes the throat location and E is for the effective values of p, M, and A. Rearranging Eq. (9) and relating the p and T values back to the nozzle intlet (they cannot be directly related to the stagnation quantities because the system is now considered to be anisentropic) provides

$$\dot{m}_a = p_{\text{in}} [\zeta_{\text{in}}/\zeta_2]^{\Gamma - \frac{1}{2}} [\psi_{\text{in}}/\psi_2]^{\lambda} M_2^E A_2^E \sqrt{\gamma/RT_1} \tag{10a}$$

where

$$\psi = 2\tan\beta - f\gamma M^2, \qquad \Gamma = \gamma(f + 2\tan\beta)/2\phi$$

$$\lambda = (f\gamma - 2\tan\beta)/2\phi, \qquad \phi = f\gamma + (\gamma - 1)\tan\beta \tag{10b}$$

Were the Mach numbers defined to be equal in the ideal and actual systems at the throat, the inlet pressure ratios could not be considered equivalent for both systems. With a given set of inlet conditions for both the ideal and actual cases then, it is convenient to define the inlet pressure ratio to be equivalent in both systems. This allows for the static pressures and static temperatures to be equivalent at the nozzle inlet and related to the inlet stangnation pressure and stagnation temperature. This relation then provides

$$\dot{m}_a = p_0 \left[1 \Big/ \zeta_{\text{in}}^{\gamma/(\gamma-1)}\right] [\zeta_{\text{in}}/\zeta_2]^{\Gamma - \frac{1}{2}} [\psi_{\text{in}}/\psi_2]^{\lambda} M_2^E A_2^E \sqrt{\gamma \zeta_{\text{in}}/RT_0} \tag{11}$$

After the collection of terms, this is more clearly written as

$$\dot{m}_a = p_0 M_2^E A_2^E \left[\zeta_{\text{in}}^{\Gamma - \gamma/(\gamma-1)} \Big/ \zeta_2^{\Gamma - \frac{1}{2}}\right] [\psi_{\text{in}}/\psi_2]^{\lambda} \sqrt{\gamma/RT_0} \tag{12}$$

Because the inlet conditions are equivalent, it follows that the throat Mach achieved is unity for maximum choking. In this case, Eq. (12) for the actual flow rate can be reduced to

$$\dot{m}_a = p_0 A_2^E \frac{\zeta_{\text{in}}^{\Gamma - \gamma/(\gamma-1)}}{[1 + (\gamma - 1)/2]^{\Gamma - \frac{1}{2}}} \left[\frac{\psi_{\text{in}}}{2\tan\beta - f\gamma}\right]^{\lambda} \sqrt{\frac{\gamma}{RT_0}} \tag{13}$$

When bleeding, cooling, and leakage losses are neglected, the flow coefficient is then written

$$C_D = \frac{\dot{m}_a}{\dot{m}_i} = \left\{ p_0 A_2^E \frac{\zeta_{\text{in}}^{\Gamma - \gamma/(\gamma-1)}}{[1 + (\gamma - 1)/2]^{\Gamma - \frac{1}{2}}} \left[\frac{\psi_{\text{in}}}{2\tan\beta - f\gamma}\right]^{\lambda} \times \sqrt{\frac{\gamma}{RT_0}} \right\} \Bigg/ \left[\frac{p_0 A_{\text{in}} M_{\text{in}}}{\zeta_{\text{in}}^{(\gamma+1)/2(\gamma-1)}} \sqrt{\frac{\gamma}{RT_0}} \right] \tag{14}$$

When the terms are reduced and it is still assumed that the throat Mach is unity, Eq. (14) becomes

$$C_D = \frac{A_2^E}{A_{\text{in}} M_{\text{in}}} \frac{\zeta_{\text{in}}^{\Gamma + (1-\gamma)/2(\gamma-1)}}{[1 + (\gamma - 1)/2]^{\Gamma - \frac{1}{2}}} \left[\frac{\psi_{\text{in}}}{2\tan\beta - f\gamma}\right]^{\lambda} \tag{15}$$

which accounts for the losses through the convergent sector of the nozzle and well defines the flow coefficient. Another convenient form, when sufficient information on the convergent nozzle sector is unavailable, is to calculate both flow rates at the throat,

$$C_D = \dot{m}_a/\dot{m}_i = \left(A_t^E \Big/ A_t^G\right)\left(M_t^E \Big/ M_i\right) \times \zeta_t^{(\gamma+1)/2(\gamma-1) - \Gamma + \frac{1}{2}} \zeta_{\text{in}}^{\Gamma - \gamma/(\gamma-1)} [\psi_{\text{in}}/\psi_t]^{\lambda} \tag{16}$$

However, Eq. (16) needs to be empirically adjusted to match the experimental data. Equations (15) and (16) establish the flow coefficient as a function of the effective throat area. They are thus ideally suited to be implemented in thrust-vectoring nozzle design as well.

What can initially be observed throughout the development of the flow coefficient is the lack of dependance on the NPR. However, the experimental data show that at very low pressure ratios (NPR = 1.5) the flow coefficient is weakly dependant on the inlet pressure. Thus, any estimation from this method, which now includes terms for the Mach number M, roughness f, and angularity α, in the nozzle will be constant regardless of the NPR.

Analytical estimation of the flow coefficient has been pursued by two methods, each relying on a different principle. Method 1 is based on Eq. (16) and requires an unrealistic adjustment to fit the data. This is an inflexible method that does not allow one to chose the nozzle geometry randomly. The advantage to this method is the independence from the convergent sector of the nozzle, and it is presented for this reason.

Method 2, based on Eq. (15), allows for more flexibility in the parameters. It is dependent on the geometry of the convergent sector of the nozzle. However, no curve fitting is required to obtain a reasonable prediction. To implement method 2, a complete evaluation of the flow coefficient through calculating the various area-reduction stages in the experimental setup was not pursued. Instead, it was found that, at the final stage just before the throat, where the convergence angle is $\beta = 20$ deg, the flow coefficient ($C_D = 0.9344$) could be achieved through method 2 within about 2% of the average experimental value ($C_D = 0.9489$) for the long-nozzle configuration. Further precision is achieved through compensating for the unaccounted losses in the previous reduction stages. This is shown in the following results. The roughness for both analytical methods was $\varepsilon = 15\ \mu$m to adhere to the actual roughness of the experimental part.

Figure 4 shows the comparison of the analytical models with the numerical and experimental results for the long nozzle, followed by the error analysis in Fig. 5. The best match of the experimental data is proven to be method 2 of the analytical model. The error, beyond NPR = 2, proves to be less than 0.5%. Because of the nonlinearity of the systems, this does not remain true for method 2 with the thrust coefficient, later. Method 1, the fitted method, is well adjusted with an average error of about 1.0% beyond NPR = 2.

The numerical simulations show a slight dependency on the NPR value at NPR = 1.5. Here the flow exits subsonically, and neither the analytical nor the numerical models are sensitive enough to model the experimental flow behavior. The numerical error is calculated similar to the analytical. The numerical model shows an average error of around 4% after NPR = 2 to satisfactorily emulate the experimental data.

If one were to assume that the expansion length has no effect on the flow coefficient, method 1 would still suffice for a good flow coefficient estimation. It proves to maintain a small error of only about 1.0% for the short nozzle, as shown in Fig. 6. The behavior of method 2 is of greater interest because it is not a curve fit but is a function of the expansion angle of the nozzle. The average error in the estimation rose slightly from 0.5 to 1.0%, well within the experimental deviation tolerance.

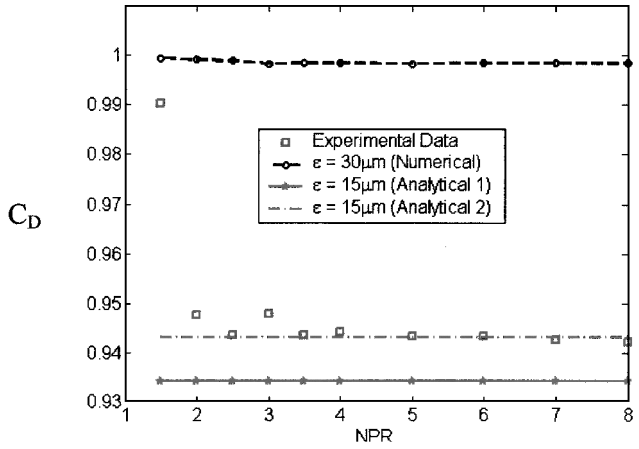

Fig. 4 Flow coefficient as a function of NPR for the long-nozzle configuration.

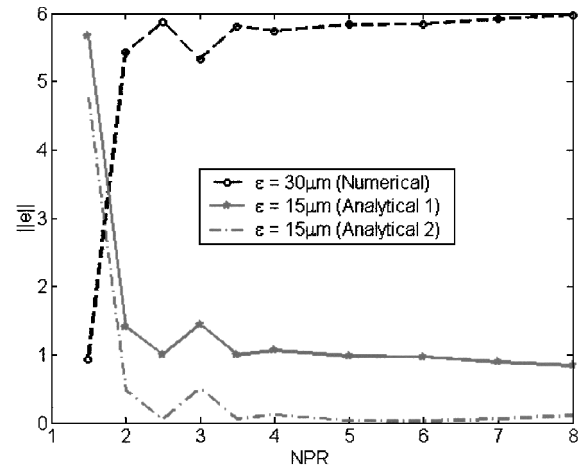

Fig. 5 Error in the predicted flow coefficient as a function of NPR for the long-nozzle configuration.

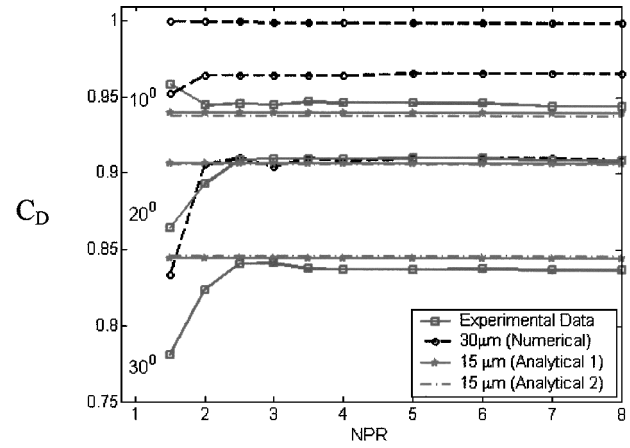

Fig. 6 Flow coefficients as a function of NPR for three vectoring angles.

Comparison between the numerical simulations and the analytical models produces an interesting result. It is apparent that the numerical simulations produce a trend opposite to that of the experimental phenomena. The numerical flow coefficient is sensitive to the NPR through the transonic exit Mach values ($1.5 \leq \text{NPR} \leq 2.0$). This sensitivity is not apparent in the analytical model. On the other hand, the analytical model is better able to achieve an estimation of the actual flow coefficient in the supersonic realm ($2.0 \leq \text{NPR} \leq 8.0$).

Thrust-Vectoring Flow Coefficient

Recalling Eq. (15), one only needs to consider that the area of the effective throat be implemented when shifting from a conventional nozzle to the vectoring of a thrust vectoring nozzle such that the calculation of the discharge coefficient remains essentially the same with the exception of the effective area ratio calculation. Figure 6 demonstrates a comparison of the numerically and analytically achieved flow coefficients.

It is shown that the analytical prediction is more precise than the numerical one in all cases. Although the apparent sensitivity to the variation in NPR at low NPR values has not been achieved in the analytical model, this result agrees with the conclusions of Gal-Or,[12] who found that the discharge coefficient is predominately a function of the nozzle angularity and practically independent of the NPR.

It was found that the numerical model overestimates the flow. If the numerical simulations were more sensitive to the roughness model, then one would expect a consistent error in the flow coefficient estimation as a function of the roughness in the model.

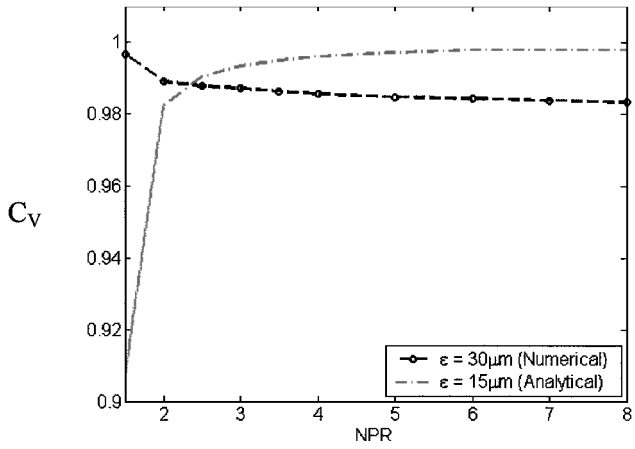

Fig. 7 Velocity coefficient for the long-nozzle configuration.

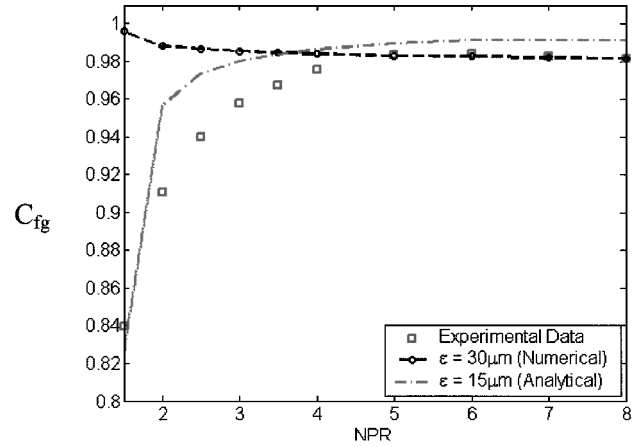

Fig. 8 Thrust coefficient as a function of NPR for the long-nozzle configuration.

Conventional Velocity Coefficient

The ratio of the actual exit velocity V_e to the ideal exit velocity V_{ei} is known as the velocity coefficient. This represents the effect of frictional loss in the boundary layer of the nozzle. It is difficult to determine experimentally because the losses for which it accounts are bound directly with the angularity losses as well (see Mattingly et al.[13] and Oates[14]). An analytical evaluation is attainable

$$C_v = V_e/V_{ei} = M\sqrt{\gamma RT}\Big/\left(M\sqrt{\gamma RT}\right)_i = (M/M_i)\sqrt{\zeta_i/\zeta} \quad (17)$$

where the gas constant R, the ratio of specific heats γ, and the stagnation temperature T_0 are considered to be constant in this adiabatic system. Thus, in the analytical model, the velocity coefficient becomes purely a function of the relation between the ideal and actual velocity values, as demonstrated in Fig. 7.

The flow through the nozzle is underexpanded until the design point is reached. After this, the flow will be overexpanded. Thus, one can expect the velocity coefficient to have a parabolic shape with a value of unity at the design point across the NPR range. In this work, the parabolic shape of the velocity coefficient is not achieved either in the analytical or the numerical model. The apparent underexpansion is modeled through a sensitivity before the nozzle design point of NPR = 5.1 is achieved. The performance peak is then achieved. The other side of the parabolic behavior is not attained because of a lack of overexpansion sensitivity in the configuration of the models.

Thrust-Vectoring Velocity Coefficient

Development and calculation of the velocity coefficient does not vary significantly during vectoring. Thus, it must suffice to restate Eq. (17) as the actual velocity over the ideal. As the effective area ratio decreases, the exit Mach number of the jet must also decrease. Although this surfaces in the numerical simulations, there is no possibility of evaluating this in the experimental data. It is only visible through secondary effects on the thrust coefficient.

Because the analytical flow evaluation produces a new design NPR each time the effective area ratio is lowered, the exit Mach at each vectoring angle for the design point is easily determined. The intermediate values are much more difficult to obtain. In this work, the intermediate exit Mach number values during vectoring are taken merely as a percent reduction of the area ratio, and the estimate achieved is satisfactory. Another possibility is to link the exit Mach number reduction to the reduction in the effective throat area.

Angularity Coefficient

Although the angularity of the exiting flow in one dimension is unity, considerations for angularity in elliptical flow can be made theoretically. Thus, angularity coefficient can be rewritten as

$$C_a = \frac{1}{A_e^G}\int_0^{2\pi}\int_0^R \left[(r_z\sin\theta)^2 + (r_y\cos\theta)^2\right]^{\frac{1}{2}} \times \cos\left[(\alpha_z\sin\theta)^2 + (\alpha_y\cos\theta)^2\right]^{\frac{1}{2}} \partial r\,\partial\theta \quad (18)$$

Conventional Thrust Coefficient

The nondimensional measure of thrust, the thrust coefficient C_{fg}, is the ratio of actual to ideal thrust. For one-dimensional flow neglecting leakage and cooling losses, it is written as follows:

$$C_{fg} = \frac{F_a}{F_i} = \frac{\dot{m}_a V_e + A_e(P_e - P_0)}{\dot{m}_i V_{ei}} \quad (19)$$

Substituting Eq. (7) and the area ratio into Eq. (19) allows for an important formulation of the thrust coefficient after the terms are separated. The thrust coefficient then becomes

$$C_{fg} = \frac{A_t^E}{A_t^G}\left\{\frac{M_a}{M_i}\sqrt{\frac{\zeta_i}{\zeta_a}} + \frac{A_e^E}{A_t^E}\frac{\sqrt{\zeta_i[(\gamma+1)/2]^{(\gamma+1)/(\gamma-1)}}}{\gamma M_i}\left(\frac{p_e}{p_a} - 1\right)\right\} \quad (20)$$

Equation (20) allows the thrust coefficient to be a function of the ratio between the effective and geometric areas of the throat. Although this value is unity in conventional axisymmetric nozzles, it bears significance later when the nozzle is vectored.

Figure 8 demonstrates the capability of the analytical model, using Eq. (20). The error analysis is shown in Fig. 9. The analytical model succeeds in modeling the trend of the thrust coefficient. It is shown to overestimate the value by about 2.0% beyond NPR = 3. Even the sensitivity of the nozzle at the lower NPR levels is shown to surface in the analytical model.

The numerical model shows very good prediction capabilities around and above the design point. It is apparent that it fails in the lower NPR values.

Thrust-Vectoring Thrust Coefficient

Equation (20) is adjusted to thrust vectoring through the considerations of the variation between the effective and geometric throat as well as of the effective area ratio on the expansion adjustment term in the braces.

Figure 10 shows the analytical prediction results for the total thrust coefficient at various vectoring angles. The error in the thrust components is a direct result of the inability to predict precisely the correct effective vectoring angle under the standard model implemented.

Below the design point NPR (5.1), the analytical model shows a slight sensitivity to the geometric vectoring angle. This is a reflection

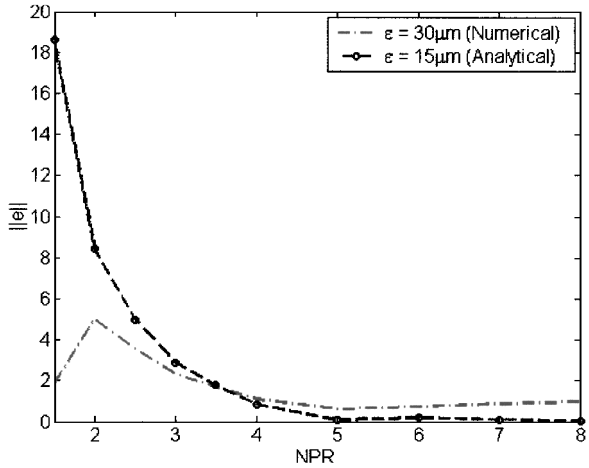

Fig. 9 Error in predicted thrust coefficient for the long-nozzle configuration.

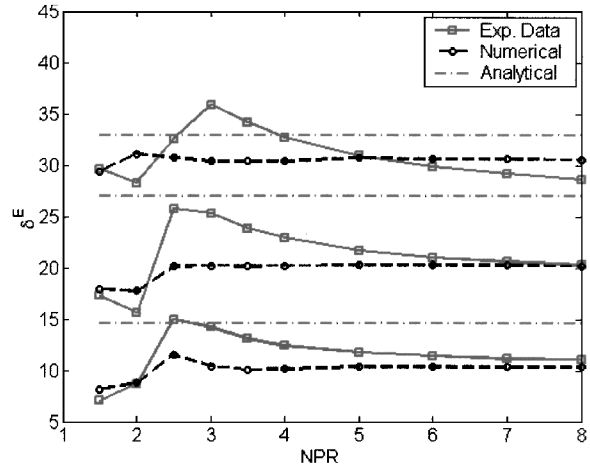

Fig. 11 Effective vectoring angle as a function of NPR.

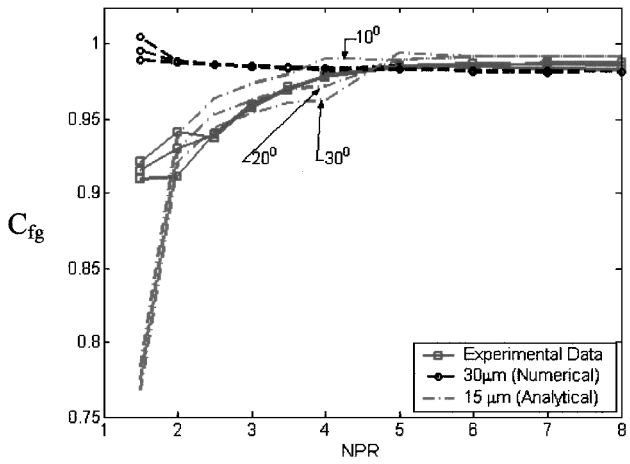

Fig. 10 Thrust coefficient as a function of NPR for three vectoring angles.

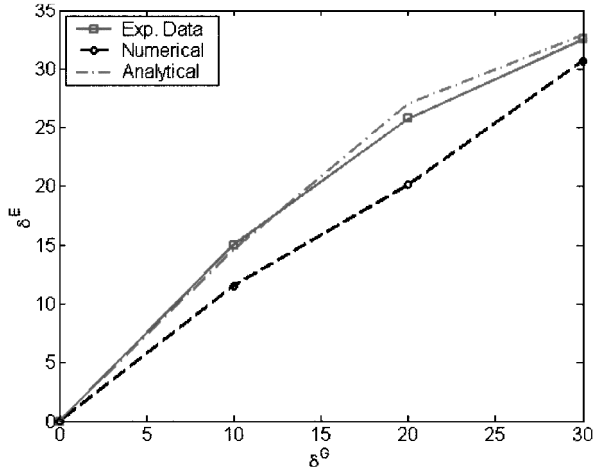

Fig. 12 Effective vectoring angles as a function of geometric vectoring angle at NPR = 2.5.

of what the data show at the lowest NPR. This sensitivity is an indication of the choking status of the nozzle in the experimental data. Although this is not true for the analytical model, there appears to be a correlation.

The numerical model shows a similar choking-dependent sensitivity at the lowest NPR values, even though at these points it is producing the largest error in its performance estimation. This error is attributable to the influence of the roughness model, which is not thoroughly appropriate in this application.

Effective Vectoring Angle

Error in the prediction of the effective vectoring angle in the numerical simulation is attributed to the turbulence intensity used as a standard throughout this work. It has been found that the flow separation after the throat on the lower-half of the nozzle directly affects the effective vectoring angle. This separation is sensitive to the turbulence intensity prescribed and, hence, so is the prediction of the effective vectoring angle.

Wilson et al.[4] have shown a geometrical prediction for the effective vectoring angle. Because of the complexity of the flow separation during vectoring, no effective vectoring angle can be determined as a function of the NPR. Thus, the prediction reduces to a pure function of the geometry. Unfortunately, this prediction is not sensitive to the NPR and, hence, produces only a straight line as seen in Fig. 11. Figure 12 shows the geometric prediction in comparison with the numerical and experimental models at NPR = 2.5. This a very favorable prediction. However, as is shown in Fig. 11, it is not the average effective angle achieved across the NPR range.

Conclusions

Implemention of the polytropic equation system as an analytical model for determining the performance coefficients in thrust-vectoring converging–diverging nozzles has been presented. The capability of this model has been contrasted with three-dimensional simulations using FLUENT and with experimental data. It has been demonstrated that the analytical model can satisfactorily predict the nozzle performances without the need for empirical data or efficiency coefficients. The numerical simulations also proved that computational fluid dynamics is a viable and useful tool for modeling in nozzle design. With the analytical model given here, not only ideal but nonideal nozzle geometries can be quickly evaluated. This system is useful in the preliminary design stage of parametric studies to determine the overall performances of a nozzle.

References

[1]Chalmers, P., "Return Flight," *Mechanical Engineering*, Dec. 1999, pp. 62–64.

[2]Gal-Or, B., "Civilizing Military Thrust Vectoring Flight Control," *Aerospace America*, No. 4, 1996, pp. 20, 21.

[3]Hienz, E., and Vedova, R., "Requirements, Definition and Preliminary Design for an Axisymmetric Vectoring Nozzle to Enhance Fighter Maneuverability," AIAA Paper 84-1212, June 1984.

[4]Wilson, E. A., Adler, D., and Bar-Yoseph, P. Z., "Geometric Evaluation of Axisymmetric Thrust-Vectoring Nozzles for Aerodynamic Performance Predictions," *Journal of Propulsion and Power*, Vol. 18, No. 3, 2002, pp. 712–715.

[5]Reynolds, M. S., Gilbert, M., and Young, F. M., "Comparison of Certain Empirical Parameters for Conical Nozzles and Diffusers with the Results of One-Dimensional Combined Change Analytical Model," *Technologies in*

Reactor Safety, Fluid Structure Interaction, Sloshing and Natural Hazards Engineering, ASME American Society of Mechanical Engineers, Fairfield, NJ, PVP-Vol. 366, 1998, pp. 309–316.

[6]Young, F. M., "Generalized One-Dimensional, Steady, Compressible Flow," *AIAA Journal*, Vol. 31, No. 1, 1993, pp. 204–208.

[7]Rebolo, R., Arrendondo, P., Matesanz, A., Velazquez, A., and Rodriguez, M., "Aerodynamics Design of Convergent-Divergent Nozzles," AIAA Paper 93-2574, June 1993.

[8]Shapiro, A. H., *The Dynamics and Thermodynamics of Compressible Fluid Flow*, Ronald, New York, 1953, pp. 60–95.

[9]Gephart, P. M., Gross, R. J., and Hochstein, J. I., *Fundamentals of Fluid Mechanics*, 2nd ed., Addison Wesley Longman, Reading, MA, 1992, pp. 483, 511.

[10]Cebeci, T., and Bradshaw, P., *Momentum Transfer in Boundary Layers*, Hemisphere, New York, 1977, pp. 1–250.

[11]Carson, G. T., and Capone, F. J., "Static Internal Performance of an Axisymmetric Nozzle With Multiaxis Thrust-Vectoring Capability," NASA-TM-4237, Feb. 1991.

[12]Gal-Or, B., *Vectored Propulsion Supermaneuverability and Robot Aircraft*, Springer-Verlag, Berlin, 1991, pp. 1–294.

[13]Mattingly, J. D., Heiser, W. H., and Daley, D. H., *Aircraft Engine Design*, AIAA Education Series, AIAA, New York, 1987, pp. 1–150.

[14]Oates, G. C.; *Aerothermodynamics of Aircraft Engine Components*, AIAA Education Series, AIAA, New York, 1985, pp. 48–120.